

# Enhancement of Underwater Images With Statistical Model of Background Light and Optimization of Transmission Map

Wei Song, *Member, IEEE*, Yan Wang, Dongmei Huang, Antonio Liotta<sup>ID</sup>, *Senior Member, IEEE*, and Cristian Perra<sup>ID</sup>, *Senior Member, IEEE*

**Abstract**—Underwater images often have severe quality degradation and distortion due to light absorption and scattering in the water medium. A hazy image formation model is widely used to restore the image quality. It depends on two optical parameters: the background light (BL) and the transmission map (TM). Underwater images can also be enhanced by color and contrast correction from the perspective of image processing. In this paper, we propose an effective underwater image enhancement method for underwater images in composition of underwater image restoration and color correction. Firstly, a manually annotated background lights (MABLs) database is developed. With reference to the relationship between MABLs and the histogram distributions of various underwater images, robust statistical models of BLs estimation are provided. Next, the TM of R channel is roughly estimated based on the new underwater dark channel prior (NUDCP) via the statistic of clear and high resolution (HD) underwater images, then a scene depth map based on the underwater light attenuation prior (ULAP) and an adjusted reversed saturation map (ARSM) are applied to compensate and modify the coarse TM of R channel. Next, TMs of G-B channels are estimated based on the difference of attenuation ratios between R and G-B channels. Finally, to improve the color and contrast of the restored image with a dehazed and natural appearance, a variation of white balance is introduced as post-processing. In order to guide the priority of underwater image enhancement, sufficient evaluations are conducted to discuss the impacts of the key parameters including BL and TM,

and the importance of the color correction. Comparisons with other state-of-the-art methods demonstrate that our proposed underwater image enhancement method can achieve higher accuracy of estimated BLs, lower computation time, overall superior performance, and better information retention.

**Index Terms**—Quality of experience, image quality, underwater image enhancement, image restoration, statistical model of background light, transmission map optimizer, color improvement.

## I. INTRODUCTION

UNDERWATER image quality enhancement is a research area fundamental for improving the quality of experience (QoE) in advanced marine applications and services. Scene understanding, computer vision, image/video compression and transmission, underwater surveillance, are some applications and services strongly depending on the availability of high-quality input images for addressing professional and consumer expectations concerning QoE.

During media acquisition in the air, poor and varying illumination conditions can drastically change image contrast and visibility [1]. The quality degradation is even higher for underwater media acquisition considering the additional physical complexity of the water compared to the air. In particular, images restoration and enhancement methods are challenging due to the complex underwater environment where images are degraded by the influence of water turbidity, light absorption, and scattering [2]. In open waters, the red light with longer wavelength than green and blue lights is attenuated faster, so that underwater images often appear with a green-bluish tone. Coastal waters with high concentrations of phytoplankton appear green and not clear, due to the light scattering by the plant and the absorption of the shortest wavelengths (blue and violet) by Chlorophyll-a [3]. The interactions among the light, the transmission medium and the scene can produce fuzzy images. McGlamery [4] and Jaffe [5] proposed a model of underwater imaging, which can be represented as a linear superposition of a direct component, a forward scattering component, and a back scattering component [6]. Several methods have been proposed to measure and enhance the perceived QoE, and in particular blind image quality assessment methods are of much interest since they do not require prior knowledge of the original content and

Manuscript received December 14, 2018; revised May 8, 2019 and September 2, 2019; accepted December 15, 2019. This work was supported in part by the National Natural Science Foundation of China under Grant 61702323 and Grant 61972240, in part by the Program for Professor of Special Appointment at Shanghai Institutions of Higher Learning under Grant TP2016038, and in part by the Italian Ministry of University and Research, within the Smart City Framework under Project PON04a2\_00381 “CAGLIARI2020.” (Corresponding authors: Yan Wang; Dongmei Huang.)

Wei Song is with the College of Information Technology, Shanghai Ocean University, Shanghai 201306, China (e-mail: wsong@shou.edu.cn).

Yan Wang is with the Academy for Engineer and Technology, Fudan University, Shanghai 201306, China (e-mail: 19110860017@fudan.edu.cn).

Dongmei Huang is with the Shanghai University of Electric Power, Shanghai 201306, China (e-mail: dmhuang@shiep.edu.cn).

Antonio Liotta is with the School of Computing, Edinburgh Napier University, Edinburgh EH10 5DT, U.K. (e-mail: a.liotta@napier.ac.uk).

Cristian Perra is with the Department of Electrical and Electronic Engineering, University of Cagliari, 09123 Cagliari, Italy, and also with CNIT Research Unit, CNIT (National Inter-University Consortium for Telecommunications), 09100 Cagliari, Italy (e-mail: cperra@ieee.org).

Color versions of one or more of the figures in this article are available online at <http://ieeexplore.ieee.org>.

Digital Object Identifier 10.1109/TBC.2019.2960942

can be easily deployed in practical visual communication systems [7], [8], [9].

Underwater images are enhanced and/or restored mainly by two kinds of algorithms and/or techniques which include image-based methods and physics-based methods [10]. The former methods modify image pixel values via image processing to improve the contrast and brightness of hazy images. Traditional image enhancement methods (e.g., White Balance, Histogram Equalization (HE), Contrast Limited Adaptive Histogram Equalization (CLAHE) [11] and improved method [12]) can improve the visibility, color and natural appearance of outdoor terrestrial images. Yet, these methods are rarely effective for underwater images with complicated physical properties. Iqbal *et al.* proposed the integrated color model (ICM) [13] and the unsupervised color correction method (UCM) [14] based on histogram stretching in RGB and HSI color model to enhance the contrast and color of the image. Ancuti *et al.* [15] proposed the fusion-based images enhancement method, which is focused on color and contrast treatment. Ghani and Isa [16], [17] improved the ICM method by stretching the input image based on the Rayleigh distribution to preserve the details of the enhanced areas.

Physics-based methods restore underwater images by considering the basic physics of light propagation in the water medium and the theory of underwater imaging. The purpose of restoration is to deduce the parameters of the physical model and then recover the underwater images by reserving compensation processing. Due to the hazing effect of underwater images caused by light degradation and scattering, similar to the effect of heavy fog in the air, He's dark channel prior (DCP) dehazing method [18] or its variations are widely used in underwater image restoration [19], [20], [21], [22]. Chao and Wang [19] directly used the DCP to recover the underwater images, but the results show a limited improvement. Chiang and Chen [21] proposed wavelength compensation and image dehazing (WCID) to remove the artificial light (AL), compensate the attenuation of each channel by the wavelength, and eliminate the effect of the haze by the DCP.

Considering the significant impact of red light on the dark channel in underwater condition, Drews *et al.* [22], [23] used DCP based on G-B channels ( $DCP_{gb}$ ) for underwater images, rather than the general DCP based on R-G-B channels ( $DCP_{rgb}$ ). Using the  $DCP_{gb}$  to obtain the transmission map could reduce the error of depth estimation. Galdran *et al.* [24] proposed a variant of the DCP which used the minimum operation of the inverted R channel and G-B channels to recover the images. Li *et al.* [25] estimated the background light by mapping the maximum intensity prior to dehaze blue-green channels and used Gray-World assumption theory to correct the red channel. Li *et al.* [26] proposed the minimal information loss principal (MILP) to estimate an optimal medium transmission map to restore underwater images. Peng *et al.* [27] considered object blurriness to estimate transmission map and scene depth. They further presented an improved method based on the image blurriness and light absorption to estimate more accurate background

light and underwater scene depth to restore a precise color image [28].

Recently, Wang *et al.* [29] proposed a generalized dark channel prior (GDCP) to calculate the difference between the original intensity and the ambient light estimated based on the depth-dependent color change. Meanwhile this method can enhance hazy, sandstorm and underwater images based on the image formation model (IFM) combining with adaptive color correction. By the analysis on statistical distribution of pixel values, Zhang *et al.* [30] proposed a non-local prior, namely, adaptive attenuation-curve prior (AACP) to estimate transmission for each pixel. In order to optimize the coarse TM, the attenuation factor and the saturation constraints are separately introduced to compensate and adjust TMs.

Carlevaris-Bianco *et al.* [31] simplified the estimation of the transmission map according to the difference between maximum values of the R channel and G-B channels, defining a maximum intensity prior (MIP) method. The above DCP-based, variations of DCP-based, MILP-based and MIP-based restoration methods using the image formation model (IFM) are not competent to the estimation of BLs and TMs under complicated underwater lighting conditions, surrounding environments and color tones. In short, physics-based methods aim to acquire more accurate TM and BL to recover underwater images.

With the development of deep learning in image restoration and enhancement, we have seen a shift from models that are completely designed by humans and optimize parameters selection to systems that are trained by computers using sample data from which feature vectors are extracted. Thus, learning-based methods for underwater image enhancement have been taken into consideration in recent years. Liu *et al.* [32] proposed the deep sparse non-negative matrix factorization (DSNMF) to estimate the image illumination to achieve image color constancy. Ding *et al.* [33] dehazed underwater images based on the depth map estimated by the Convolutional Neural Networks (CNN), which was trained with balanced images produced by adaptive color correction. Ding *et al.* [34] also introduced super-resolution CNN to remove blurring of underwater images.

In order to restore underwater images, Cao *et al.* [35] estimated background light employing a 5-layer CNN and predicted scene depth map using a multi-scale architecture, stacking two deep networks, a coarse global network and a refined network, in reference with [36]. These deep learning network models can only adapt to some limited kinds of underwater images due to the use of synthetic underwater images for training. There are many deep learning-based dehazing [37], deblurring [38], denoising [30] methods for outdoor images. However, these can not always directly be applied for underwater conditions.

More recently, some researchers have began to work on underwater images databases [39], [40]. These benchmark works will bring opportunities for developing better deep learning methods for underwater image enhancement. Nevertheless, deep learning methods are extraordinarily time consuming compared with the physical or non-physical models under the same processing circumstance.

It is challenging to effectively restore different kinds of underwater images under diverse scenarios and/or with different distortions. Existing methods of underwater image restoration either produce inaccurate estimation of the parameters of the background light (BL) intensity and transmission maps (depth maps), or have high complexity. In particular, white objects in the image, floating particles in the foreground, artificial light in the background region, or dim background light, can easily interrupt the correct estimation of BLs and TMs based on present state-of-the-art restoration methods. Ignoring light selective attenuation under the water also impacts the estimation accuracy of BL and TM.

In this paper, we propose an effective and robust underwater image restoration method based on IFM, emphasizing on fast BLs estimation based on statistical modelling and accurate TMs estimation based on new underwater dark channel prior and the optimizer of the depth map and Reversed Saturation Map (RSM). We use color correction (CC) as a key post-processing to enhance the contrast and visibility of the restored images. The contributions of this paper are summarized as follows:

a) A MABLs database is established with 500 underwater images. The manual annotation was based on the general concept of “background light”, that is, the light used to illuminate the background area. In order to guarantee the availability, MABLs are selected from one thousand BLs estimated manually after removing some unreliable BLs with latent errors or uncertain elements. Finally, the database has proved to be highly accurate in terms of the good recovered quality of various underwater images using the MABLs. To the best of our knowledge, this is the first database for underwater image BL estimation.

b) A novel model of the background light estimation is proposed based on the statistical analysis of the distribution characteristics of each R-G-B channels, which is built on the combination of the average value, the median value and the standard deviation of each channel distribution. Compared with other recent BL estimation models, our statistical model can improve the accuracy and be significantly time-saving without any prior information about the underwater images.

c) An optimal model of TM estimation. The TM of the R channel is derived based on a new underwater dark channel prior conforming to the distribution characteristics of HD underwater images, and combine with the compensation of the depth map and the optimization of the RSM. The TMs of G-B channels are constructed by considering the difference of attenuation rates between R and G-B channels in underwater environments. The proposed TM model can achieve superior results to the state-of-the-art models, at lower complexity.

d) An enhancement method for different underwater images is given in two steps: (i) image restoration using the IFM model with the proposed BL estimator and TM optimizer; (ii) image color correction with a modified white balance algorithm. This method successfully improves the quality of underwater images by adequately taking advantages of both the physics-based method and the image processing method.

e) Comprehensive experiments and assessments are conducted in this paper to deliver fair and sufficient evaluations

and discussions of the impact on the key parameters BL and TM, and underwater images enhancement quality, involving other state-of-the-art methods.

f) The above mentioned MABLs database and the proposed BL and TM estimation algorithms are available online.<sup>1</sup>

The remainder of the paper is organized as follows. Section II presents the related work. The proposed method is described in Section III. The obtained results are reported in Section IV. Section V provides a discussion of the findings. Conclusions are drawn in Section VI.

## II. RELATED WORK

### A. Image Formation Model

A simplified image formation model (IFM), often used to approximate the propagation equation of underwater scattering ([24], [41], [42], [43], [44]) is described as:

$$I^c(x) = J^c(x)t^c(x) + (1 - t^c(x))B^c, c \in \{r, g, b\} \quad (1)$$

where  $c$  represents one of red, green or blue color channels;  $I^c(x)$  and  $J^c(x)$  are, respectively, the captured and restored radiance of the pixel point  $x$  in one channel  $c$ ;  $B^c$  represents the intensity of the global background light (BL), i.e., three values corresponding to R-G-B channels;  $t^c(x) \in (0, 1)$  describes the residual energy ratio after the scene radiance reaches the camera.

The values of  $t^c(x)$  for an entire image can form a transmission map (TM), which describes the portion of the scene radiance that is not scattered or absorbed and reaches the camera. The function  $t^c(x)$  can be expressed as an exponential decay function depending on the scene depth  $d(x)$  and on the spectral volume attenuation coefficient  $\beta(x)$  [45], that is:

$$t^c(x) = e^{-\beta(x)d(x)} = Nrer(c)^{d(x)}, c \in \{r, g, b\} \quad (2)$$

where  $e^{-\beta(x)}$  can be represented as the normalized residual energy ratio  $Nrer(c)$ , which depends on the wavelength of one channel and the water type. Yet, approximately 98% of the world's clear oceanic or coastal water (ocean type I) follows the rule [3], where accredited ranges of  $Nrer(c)$  in R-G-B light are 80%~85%, 93%~97%, and 95%~99%, respectively.

### B. Background Light Estimation

In order to facilitate the description, throughout this paper  $c$  denotes one of the R-G-B channels and  $c'$  denotes one of the G-B channels;  $\Omega$  denotes a local patch, whose size is  $9 \times 9$  pixels, unless specified otherwise. The simplest method for background light (BL) estimation is based on the brightest pixel in the whole underwater image. This is often not applicable to the scenarios where the foreground objects are brighter than the global background light. To reduce the impact of suspended particles in the image,  $DCP_{rgb}$  based methods [20], [21] choose the pixel located at the brightest point in the dark channel of the image to estimate BLs, that is:

$$B^c = I^c \left( \operatorname{argmax} \left( \min_{y \in \Omega} \left( \min_c I^c(y) \right) \right) \right). \quad (3)$$

<sup>1</sup><https://github.com/wangyanckxx/Enhancement-of-Underwater-Images-with-Statistical-Model-of-BL-and-Optimization-of-TM>.

To eliminate the effect of the red channel, the BLs are selected by finding the brightest pixel from only the green and blue channels,  $DCP_{gb}$  [22], where  $I^c(y)$  in the Eq. (3) is replaced with  $I^{c'}(y)$ . Meanwhile the  $B^c$  is selected as the brightest pixel or the average value of the top 0.1% brightest pixels in  $DCP_{rgb}$  [20] or  $DCP_{gb}$  [46].

The BLs can also be estimated by selecting the maximum difference between R and G-B channels in the input image, considering the fact that the red channel attenuates much faster than green and blue channels in underwater images [31]:

$$B^c = I^c \left( \text{argmax} \left| \max_{y \in \Omega} I^r(y) - \max_{y \in \Omega} I^{c'}(y) \right| \right) \quad (4)$$

A quad-tree subdivision algorithm was proposed to estimate the BL based on the higher score of the average pixel value, subtracted by the standard deviation within the pure image region [47]. This algorithm firstly divides the input image into four rectangular regions, then searches for the flat background region with highest score, and finally uses Eq. (4) to decide the final BLs.

A more complex BLs estimation is based on multiple BL candidates selection [28]. Three BL candidates are the top 0.1% blurry pixels in the input image, the lowest variance region and the largest blurriness region [27]. To compute blurriness, an initial image blurriness map  $P_{init}$  is computed as:

$$P_{init}(x) = \frac{1}{n} \sum_{i=1}^n |I_g(x) - Gau^{r_i, r_i}(x)| \quad (5)$$

where  $I_g$  is the grayscale of the input image  $I^c$ ,  $Gau^{r_i, r_i}(x)$  is the input image filtered by a  $r_i \times r_i$  spatial Gaussian filter with variance  $r_i^2$ ,  $r_i = 2^i n + 1$ , and  $n$  is set to 4. Next, the max filter is used to calculate the rough blurriness map  $P_r$  as:

$$P_r = \max_{y \in \Omega} P_{init}(y) \quad (6)$$

where  $\Omega$  is set as the size of  $5 \times 5$  pixels for the test image of  $400 \times 600$  pixels in [27], [28]. The  $P_r$  is refined by filling the holes caused by flat regions in the objects, using morphological reconstruction, and the guided filter smoothing. The refined blurriness maps  $P_{blr}$  is defined as

$$P_{blr}(x) = F_g\{C_r[P_r(x)]\} \quad (7)$$

From the blurriness map, the BL candidates are determined, of which the regions are obtained by iteratively dividing the input image into four same-size regions, using quad-tree decomposition. Because the image under sufficient light has a brighter BL, the weighted combination of the maximum and minimum candidate BLs is used to acquire the final BL, as

$$B^c = \alpha \times B_{max}^c + (1 - \alpha) \times B_{min}^c \quad (8)$$

where  $\alpha$  is selective coefficient,  $B_{max}^c$  and  $B_{min}^c$  are the maximum and minimum candidate BLs, respectively.

### C. Transmission Map Estimation

The DCP firstly proposed by He *et al.* [18], considered that in most of the non-sky patches at least one pixel of RGB channels in the local patch has an extraordinarily-low (almost zero)

intensity on the statistical prior of outdoor haze-free images. This is described as:

$$J_{dark}^{rgb}(x) = \min_{y \in \Omega^{min}} \left\{ \min_c J^c(y) \right\} = 0 \quad (9)$$

Applying the minimum filter to both sides of Eq. (1), and dividing by  $B^c$ , we can get:

$$\min_{y \in \Omega} \left\{ \min_c \frac{I^c(y)}{B^c} \right\} = \min_{y \in \Omega} \left\{ \min_c J^c(y) \right\} + 1 - t_{DCP}(x). \quad (10)$$

Substituting Eq. (9) into Eq. (10),  $t_{DCP}(x)$  is expressed as:

$$t_{DCP}(x) = 1 - \min_{y \in \Omega} \left\{ \min_c \frac{I^c(y)}{B^c} \right\}. \quad (11)$$

Due to the aggressive attenuation of the red channel in underwater images, the  $DCP_{gb}$  that considers only G and B channels was defined as underwater DCP (UDCP) [22], [23]. Then,  $t_{UDCP}(x)$  [22] can be obtained by replacing  $I^c(y)$  with  $I^{c'}(y)$ . The maximum intensity prior (MIP) [31], calculating the difference between the maximum intensity of the R channel and that of G-B channels, is used to estimate the transmission map, described as the following:

$$\begin{cases} D_{mip}(x) = \max_{y \in \Omega} I^r(y) - \max_{y \in \Omega} (I^{c'}(y)) \\ t_{MIP}(x) = D_{mip}(x) + 1 - \max(D_{mip}(x)). \end{cases} \quad (12)$$

Differently from the above methods, the scene depth is estimated by combining three depth maps including the maximum filter of red channel  $d_R$ , the maximum intensity  $d_D$  and the image blurriness  $d_B$ , as

$$d_n = \theta_b[\theta_a d_D + (1 - \theta_a)d_R] + (1 - \theta_b)d_B \quad (13)$$

where  $\theta_a = s(\text{avg}_c(B^c), 0.5)$  and  $\theta_b = s(\text{avg}_c(I^r), 0.1)$  are determined by a similar sigmoid function. After the relative depth map is refined by guided filtering [48], the final scene depth  $d_f$  is obtained by transforming the relative distance to the actual distance. The TM for the red channel is calculated as:

$$t^r(x) = e^{-\beta^r d_f} \quad (14)$$

where  $\beta^r \in \left(\frac{1}{8}, \frac{1}{5}\right)$  following [21], [49] and the TMs of G-B channels are obtained considering the attenuation ratios of G-B channels with respect to R channel [45].

## III. PROPOSED METHOD

Our method works in the R-G-B color space, aiming to not only recover the underlying scene radiance but also improve the contrast, color and visibility. The flowchart of our proposed method is shown in Fig. 1. We firstly propose effective statistical models to estimate the overall background lights (BLs) of R-G-B channels. Then, we estimate the transmission maps (TMs) of R-G-B channels based on the new UDCP integrated with TM optimizer, and the exponential decay function of three channels. Applying the estimated BLs and TMs into the underwater IFM, we gain a dehazed image. Finally, we further correct the brightness and color of the restored image via a simple color correction with white balancing using the optimal gain factor.

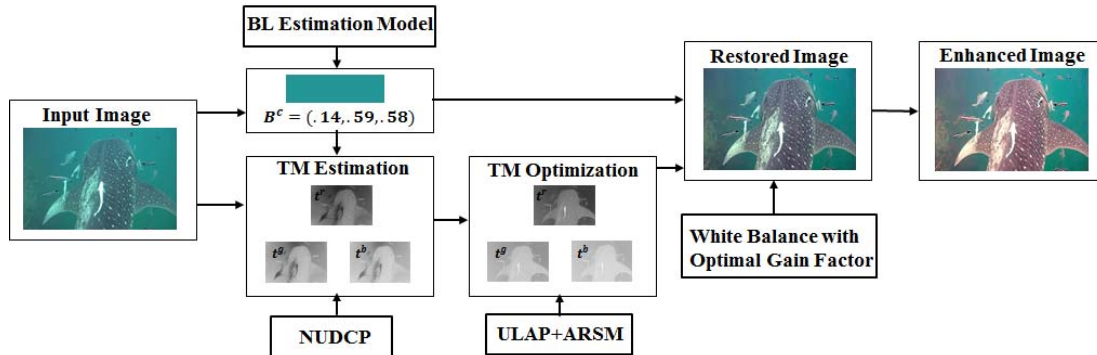


Fig. 1. Flowchart of the proposed method.

### A. Background Light Estimation Model

The existing BL estimation methods based on DCP or its variations [18], [20], [22], the hierarchical searching method [19], [26] or the BL candidate selection [28], have relatively high computation complexity and just perform well for some specific underwater scenes. In this paper, according to BL selection mechanism, we establish the first manually annotated background lights database (MABLs). Then, based on the MABLs, we proposed linear and non-linear models for BL estimation of R channel and G-B channels. And the effectiveness of proposed MABLs and the accuracy of our proposed BL estimation model are expressed in Section V.

1) *Manually Annotated Background Lights (MABLs)*: Despite the many BL estimation methods, no one has provided an objective assessment of the accuracy of BL estimation, due to the lack of the “accurate” BLs. In this paper, we establish the first dataset of BLs for underwater images, which will serve as an important benchmark to support the related research. The dataset consists of manually annotated background lights values for 500 underwater images, hereinafter referred to as MABLs. Firstly, we collect over 2000 underwater images from a range of papers ([5], [12], [15], [16], [19], [21], [22], [27], [50], [50]) and from the YouTube, Google Images and Flickr. These underwater images are manually resized to the uniform  $400 \times 600$  pixels. Among these images, to ensure the diversity of the database, we randomly select 1000 images based on the following criteria: (1) various underwater scenes, including single fish, shoal of fish, coral, diving, and underwater archaeology, and (2) different distortions such as deep-water, low-visibility, thickly hazed, greenish-bluish, noise, turbid scenes. Around 50% of samples are discarded during the process of validity measurement. These guaranteed MABLs are retained as the final MABLs database. Although our database with 500 underwater images is limited, it is still significantly valuable, given that public database of underwater images is very few (most databases include outdoor images) and no such manually annotated BLs are available.

When annotating the BLs, we invited 15 participants (10 males and 5 females) from Shanghai Ocean University, who are in their twenties, non-experts but have a proper understanding on the visual images. For 2000 hazy and coarse underwater images, the subject was asked to select the position of background light and record the corresponding pixel values

Fig. 2. Some samples and the corresponding MABL normalized in the  $[0, 1]$  range.

on each underwater image, in compliance with the principle of choosing the far scene point with high intensity. The principle represents the general concept of “background light”: the light used to illuminate the background area. Then, from the twenty selected points of each image, we chose the one with the largest difference between R and G-B intensities and got its intensity value as the final annotated BLs. This follows the principle of underwater optical imaging: because the R light attenuates much faster than the G and B lights in water, the difference between R and G-B should be bigger when the light travels from the far point to the camera. Finally, we employed five professionals with a strong background in image/video processing or computer vision, to assess the above estimated BLs by our participants and give some valuable suggestions about improving the MABLs.

We found the feasible rules to manually estimate the BLs. Yet, the participants and even the professionals failed to annotate BLs for one third of underwater images under complicated conditions, such as in close-up scenes. Hence, we firstly discarded those images that cannot be annotated manually. Abiding by the rule of the minority subordinated to the majority, we filtered out the candidates for which fewer than three professionals approved the BLs selected by the other participants. Finally, we selected 500 underwater images with reliable BLs and from different types as the MABLs, and split the dataset into training and testing data in a ratio of 7:3. Fig. 2 shows some samples of the underwater images and the corresponding MABLs, which are normalized to the range of  $[0, 1]$ .

2) *Statistical Model for BL Estimation*: Based on the training data of MABLs, we propose a simple but effective model for BL estimation via statistical analysis. We have discovered the tight correlations between the MABLs values and the histogram distribution characteristics of the underwater images, in different R-G-B color channels. Fig. 3 gives examples of five

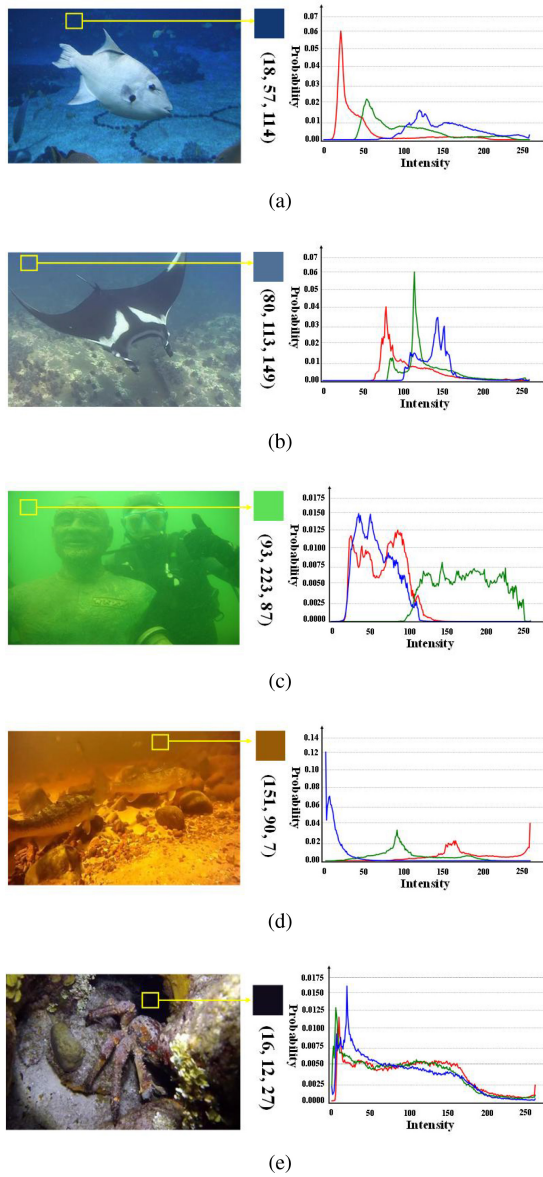


Fig. 3. Underwater images with five typical underwater scenes and the tight relationship between MABLs and the histogram distribution.

typical underwater scenes, to show how the trends of histogram vary within different BLs. The red, green and blue lines in the histograms correspond to the probability distributions of R, G, and B channels, respectively.

For instance, in Fig. 3(a) and (b), the median values of R-G-B channels in the histogram are very close to the MABLs of the images. They are not affected by the large white regions in the front of the image, which can be misestimated as the BL candidate by the DCP-based, UDCP-based BL estimation algorithms that consider the brightest region under the dark channel maps of RGB channels or GB channels as the background area. In Fig. 3(c), the green is distributed with much higher intensities than the red and blue. While in Fig. 3(d), the red dominates the background light. Fig. 3(e) has a near-black background light and its R-G-B distribution is consistent. To seek for the relationship between the MABLs and the characteristics of R-G-B histogram distribution, we investigated

TABLE I  
PEARSON CORRELATION COEFFICIENTS (PCC) AND SPEARMAN COEFFICIENTS (SPC) BETWEEN MABLs AND THE AVG, MED, MAX, MIN AND STD IN CORRESPONDING TO EACH R-G-B CHANNEL

Channel	Avg	Med	Max	Min	Std
R	0.824**	0.844**	0.269**	0.639**	0.216**
G	0.687**	0.672**	0.017**	0.264**	0.186**
B	0.742**	0.719**	0.274**	0.149**	0.405**

\*\* Coefficient is significant at the 0.01 level (2-tails).

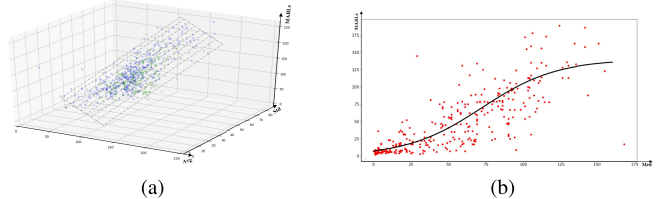


Fig. 4. Scatter plots between MABLs and the model parameters. (a) B and G channels, (b) R channel.

the following parameters: the average value (Avg), the median value (Med), the maximum value (Max), the minimum value (Min) and the standard deviation (Std), which fully express the relatively-concentrated distribution components in each color channel of an underwater image.

Pearson correlation analysis between these parameters and MABLs were run for G-B channels, and Spearman correlation analysis was performed for R channel, since the distributions of MABLs and the investigation parameters in the R channel are not normal. The normality was examined by Shapiro-Wilk test  $sig > 0.05$  after removing some outliers. Both correlation coefficient ranges are  $(-1, 1)$ . Worth recalling that Pearson coefficients (PCC) close to 1 or  $-1$  indicate a perfectly linear relationship, whereas values close to 0 demonstrate no relations. Spearman coefficients of 1 or  $-1$  indicate a perfect monotonic relationships between two variables.

Table I shows the correlation coefficients. We further investigated the correlations within these parameters, in order to eliminate the redundant ones. Due to the significantly strong correlation between Avg and Med ( $r > 0.8, p < 0.001$ ), only one of them was chosen as the predictor, that was Med for the R channel, and Avg for the G-B channel. For the R channel, we removed the redundant parameters Max and Min, because of the strong correlations between Min and Med ( $r = 0.677, p < 0.001$ ) and between Max and Std ( $r = 0.783, p < 0.001$ ). For the B channel, Std had a significantly higher correlation than Max and Min, thus it was selected. For the G channel, we also chose Std in order to stay consistent with the B channel, and because of the high correlations between Std and Max ( $r = 0.594, p < 0.001$ ) and between Std and Min ( $r = -0.674, p < 0.001$ ).

Fig. 4 demonstrates the relationships between the MABLs and the selected parameters. According to the relation of the selected parameters and the MABLs, firstly we define a linear model of the Avg and the Std for the BL estimation of the G-B channels, as follows:

$$B^{c'} = \alpha \times Avg^{c'} + \beta \times Std^{c'} + \gamma \quad (15)$$

where  $Avg^{c'}$  and  $Std^{c'}$  are the average and the standard deviation of channel  $c'$  of the input image, respectively;  $\alpha$  and  $\beta$

are coefficients;  $\gamma$  is a constant. The linear regression model for capturing the correlation between MABLs of G-B channels and the two selected parameters is chosen because it is simple but sufficient for our purposes.

As for R the channel, a non-linear model is defined in (16) based on curve estimation.

$$B^r = \frac{a}{1 + b \times \text{Exp}(c \times \text{Med}_r)} \quad (16)$$

where a, b, c are the coefficients. To avoid the effect of noise or extreme values of pixels, we used the middle 80% of the entire channel intensity histogram of coarse underwater images (limited to 10% from the lower and upper parts) to calculate the Avg, Med and Std. Through linear regression and non-linear regression under 10-fold cross validations, we eventually determined these coefficients in Eq. (17) and Eq. (18), as:

$$B^{c'} = 1.13 \times \text{Avg}^{c'} + 1.11 \times \text{Std}^{c'} - 25.6 \quad (17)$$

$$B^r = \frac{140}{1 + 14.4 \times \text{Exp}(-0.034 \times \text{Med}_r)} \quad (18)$$

We used the coefficient of determination  $R^2$  and adjusted  $R^2$  (for the number of predictor variables) to represent the goodness of fit of these regression models.  $R^2 = 1 - \text{the sum of squared error}/\text{the sum of squared total}$ , which means that the model accounts for the amount of variability in BLs. For the linear model (17), the Adjusted  $R^2$  is above 0.6. For the non-linear model (18),  $R^2$  is above 0.65.

To avoid producing over or under estimated BLs due to the limited MABLs, we restricted the value of the estimated BLs between 5 to 250. In practice, zero value of BLs is not advisable because BLs will be used as the denominator when estimating TMs. Meanwhile, due to light absorption, BLs usually cannot reach the maximum value of 255. Therefore, the final estimated BLs are as follows:

$$B^c = \min(\max(B^{c',r}, 5), 250), c \in \{r, g, b\}. \quad (19)$$

### B. Transmission Map Estimation Model

Due to the similarities between the outdoor haze images and the underwater images, the TMs are often estimated using DCP [18], [19] and its variation UDCP [22], which were under the assumptions of  $J_{dark}^{rgb} = 0$  and  $J_{dark}^{gb} = 0$ , respectively. Although the DCP and UDCP assumptions seem proper, using them for underwater images would arise some problems because they both ignored the wavelength independence in the water medium. Inspired by the process of He *et al.* [18] finding the dark channel prior from the outdoor images, we proposed a new underwater dark channel prior (NUDCP) based on the statistics of high-quality underwater images. We first selected some clear and high resolution underwater images (not less than  $1280 \times 720$  pixels) from Google Images, shutterstock.com, and pixabay.com, including underwater animals, various marine scenes, coral reefs, rocks, archaeological ruins and divers.

Some clear underwater images are shown in Fig. 5. In order to verify our prior of underwater images, all selected images were resized to  $400 \times 600$  pixels and their dark channels were



Fig. 5. Samples of our high-quality underwater images.

computed using the local patch size of  $13 \times 13$  pixels, following the process described in [18].

500 haze-free underwater images were used for computing the histograms and cumulative distributions of pixel values. Fig. 6 shows the statistics results of the R-G-B dark channel ( $DCP_{rgb}$ ) and G-B dark channel ( $DCP_{gb}$ ) based on our high-quality underwater images database. Each bin in Fig. 6(a) and (c) stands for 16 pixel intensities in an interval of (0, 255).

Although the distributions of Fig. 6(a-b) show a similar distribution shape to that of outdoor image DCP [18], the ratios of zero values in our distributions are much lower. Our statistical results on the R-G-B channels show the probabilities of 0, (1, 15), (16, 47) are approximately 40%, 20% and 20%, respectively. Instead, the statistics achieved by He *et al.* [18] showed that about 75% of the pixels were 0, and 90% were below 25.

From the distributions of Fig. 6(c-d), we can observe an even lower probability of zero values, which violates the assumption of DCP proposed by He *et al.* Therefore, we argue that it is inappropriate to simply set  $J_{dark}^{rgb}(x)$  or  $J_{dark}^{gb}(x)$  to 0 for underwater images.

Given that about 70% of underwater dark channel pixels are located between 0 and 25, we suggest the value of underwater dark channel prior could be set to 25. After normalization, we set  $J_{dark}^{gb} = 0.1$  as the result of NUDCP.

Firstly, we take the minimization operation in the local patch  $\Omega$  on the unclear underwater image in Eq. (1):

$$\min_{y \in \Omega}(I^c(y)) = \min_{y \in \Omega}\{J^c(y)t^c(y)\} + \min_{y \in \Omega}\{(1 - t^c(y))B^c\} \quad (20)$$

As the background light is homogeneous and the estimated BL is greater than 0 (as shown in Eq. (19)), both sides of Eq. (18) can be divided by  $B^c$ :

$$\frac{\min_{y \in \Omega}(I^c(y))}{B^c} = \frac{\min_{y \in \Omega}(J^c(y)t^c(y))}{B^c} + \min_{y \in \Omega}(1 - t^c(y)) \quad (21)$$

The TM is essentially constant on the small local patch; thus, Eq. (19) can be expressed as:

$$\frac{\min_{y \in \Omega}(I^c(y))}{B^c} = \frac{\min_{y \in \Omega}(J^c(y))}{B^c}t^c(x) + (1 - t^c(x)) \quad (22)$$

The final minimum filter is performed among three color channels as follows:

$$\min_c \left\{ \frac{\min_{y \in \Omega}(I^c(y))}{B^c} \right\} = \min_c \left\{ \frac{\min_{y \in \Omega}(J^c(y))}{B^c}t^c(x) \right\} + 1 - \min_c \{t^c(x)\} \quad (23)$$

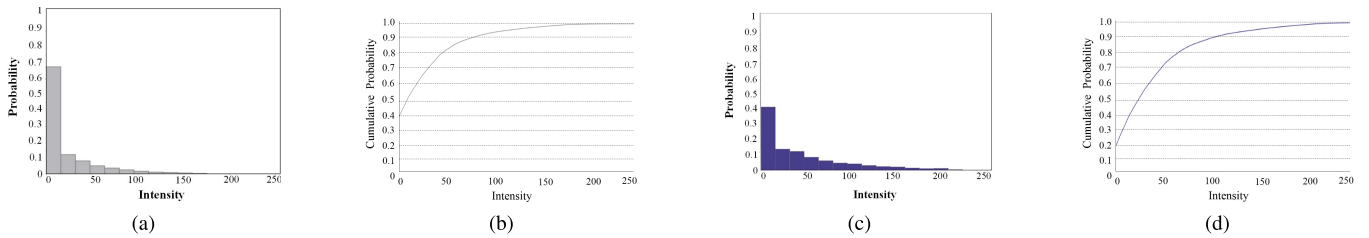


Fig. 6. Statistics of the R-G-B dark channel and the G-B dark channel, based on our high-quality underwater images database. (a) Histogram distribution of the R-G-B dark channel (each bin stands for 16 intensity levels), (b) Cumulative distribution of the R-G-B dark channel, (c) Histogram distribution of the G-B dark channel, (d) Cumulative distribution of the G-B dark channel.

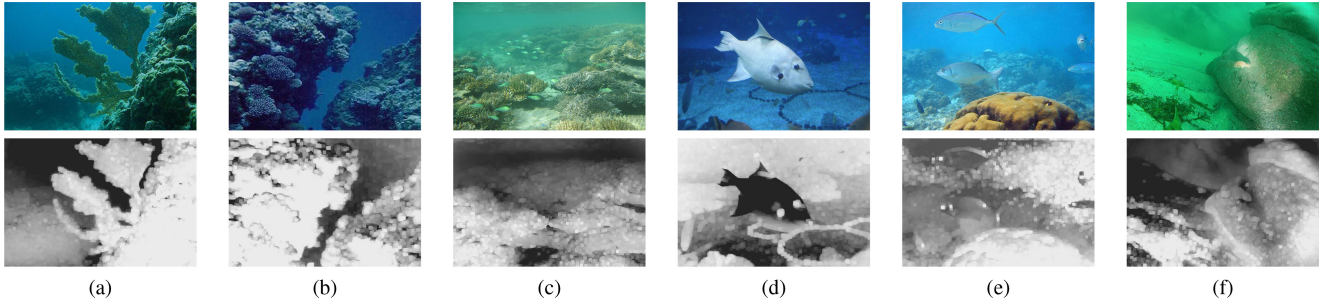


Fig. 7. Some typical underwater images (top row) and corresponding TMs of the red channel (bottom row), based on the assumption of new UDCP. (a)–(c) For the images with the dim foreground and light background, we obtain accurate TMs. (d)–(f) Influenced by the white fish, the relatively low intensity of red channel, and the artificial light shot in the foreground stone, the estimates are apparently incorrect TMs.

The first term on the right-hand side of Eq. (23) can be expressed with the following equality:

$$\min_c \left\{ \frac{\min_{y \in \Omega}(J^c(y))}{B^c} t^c(x) \right\} = \min_c \left\{ \frac{\min_{y \in \Omega}(J^c(y))}{B^c} \right\} \times \min_c \{t^c(x)\} \quad (24)$$

The first term on the right-hand side of Eq. (24), labelled as  $V$ , can be expressed as the following inequality:

$$\frac{\min_c \{ \min_{y \in \Omega}(J^c(y)) \}}{\max_c \{ B^c \}} \leq \min_c \left\{ \frac{\min_{y \in \Omega}(J^c(y))}{B^c} \right\} = V \leq \frac{\min_c \{ \min_{y \in \Omega}(J^c(y)) \}}{\min_c \{ B^c \}} \quad (25)$$

Because of  $\min_c \{ \min_{y \in \Omega}(J^c(y)) \} = 0.1$  based on our NUDCP, the following inequality holds:

$$\frac{0.1}{\max_c \{ B^c \}} \leq V \leq \frac{0.1}{\min_c \{ B^c \}} \quad (26)$$

According to  $t_\lambda(x) = Nrer(\lambda)^{d(x)}$  in Eq. (2), among R-G-B channels,  $Nrer(Red)$  is the lowest residual value in the same local patch. Hence  $\min_c \{ t^c(x) \}$ , can be expressed as  $t^r(x)$ , therefore, Eq. (21) can be rewritten as:

$$\min_c \left\{ \frac{\min_{y \in \Omega}(J^c(y))}{B^c} \right\} = V \times t^r(x) + 1 - t^r(x) \quad (27)$$

And  $t^r(x)$  can be obtained as:

$$t^r(x) = \left( 1 - \min_c \left\{ \frac{\min_{y \in \Omega}(J^c(y))}{B^c} \right\} \right) / (1 - V) \quad (28)$$

Meanwhile, the  $t^r(x)$  ranges from zero to one. When the bigger  $V$  is, the  $t^r(x)$  tends to be greater than 1. In order to minimize the information loss of the TM, in this paper,  $V$  is set as  $\frac{0.1}{\max_c B^c}$

and  $\max_c B^c$  is simply set as  $B_{max}$ . Finally, Eq. (26) can be rewritten as:

$$t^r(x) = \frac{1 - \min_c \left\{ \frac{\min_{y \in \Omega}(J^c(y))}{B^c} \right\}}{1 - 0.1/B_{max}} \quad (29)$$

To smooth the transmission map of the red channel in the IFM,  $t^r(x)$  is stretched to a proper range ( $O_{min}, O_{max}$ ), following the histogram stretching [51] as:

$$t_{out} = (t_{in} - t_{min}) \left( \frac{O_{max} - O_{min}}{t_{max} - t_{min}} \right) + O_{min} \quad (30)$$

where  $t_{in}$  and  $t_{out}$  are the input and output pixels of the transmission map, respectively, and  $t_{min}$ ,  $t_{max}$ ,  $O_{min}$  and  $O_{max}$  are parameters for the before and after stretched transmission map, respectively. To reduce the under- and over-stretched effects,  $t_{min}$ ,  $t_{max}$  are set to 0.2% of the lower and upper range of the TM histograms, and the  $(O_{min}, O_{max})$  is set to  $(0.1, 0.9)$ .

Using Eqs. (29) and (30), we can get coarse TMs. Some example underwater images and their red channel coarse TMs are shown in Fig. 7. According to Fig. 7(a)–(c), our proposed NUDCP can successfully estimate TMs for the underwater images that are featured by dim foreground scene and light background scene. However, in Fig. 7(d), the white fish in the foreground is regarded as the background scene, and our proposed method failed to identify the distance from the camera to a near fish and the far background. In Fig. 7(e), some regions of the TM seem overestimated because these have a relatively lower intensity of R channel than the background light, leading to a higher value of TM. Fig. 7(f) shows an artificially illuminated scene and its incorrect TM. This is because the TM is estimated based on the assumption that the light source is far from the camera, which is the opposite case when artificial light is used. These problems happen

in all DCP-based methods, including our NUDCP. Readers who are interested in other TM estimation methods, such as DCP [18], UDCP [22] and MIP [31], can find a comprehensive comparison in our recent review paper [10].

We solved these issues by the following two steps: the compensation by the depth map and the optimization by adjust reversed saturation map (ARSM).

In our previous work [52], we revealed that with underwater light attenuation prior (ULAP) the scene depth increases with the difference between the maximum value of G and B lights and the value of the R light. In other words, the difference between the maximum value of G-B intensities (simplified as MVGB) and the value of R intensity (simplified as VR) is very strongly related to the change of the scene depth. Based on the ULAP, we define a linear model of the MVGB and VR for the depth map estimation as follows:

$$d(x) = \mu_0 + \mu_1 m(x) + \mu_2 v(x) \quad (31)$$

where  $x$  represents a pixel,  $d(x)$  is the underwater scene depth at point  $x$ ,  $m(x)$  is the MVGB,  $v(x)$  is the VR. The best learning result is  $\mu_0 = 0.53214829$ ,  $\mu_1 = 0.51309827$  and  $\mu_2 = -0.91066194$ . In order to operate edge-preserving smoothing on the coarse estimated depth maps, the guided filter [48] is used to refine the depth maps.

The estimated depth maps are the relative distance in the image. To measure the absolute distance from the camera to each scene point, the distance  $d_0$  between the closest scene point and the camera must be estimated in advance. Via the maximum difference between the estimated  $B^c$  and the input image  $I^c(x)$ , the base depth  $d_0$  can be calculated by:

$$d_0 = 1 - \max_{x,c} \left( \frac{|B^c - I^c(x)|}{\bar{B}^c} \right) \quad (32)$$

where  $\bar{B}^c = \max(1 - B^c, B^c)$ ,  $d_0 \in [0, 1]$ . The denominator in Eq. (32) is used as the normalization factor. The numerator is the absolute difference between the observed intensity and the background light, and the point where the larger value is closer to the camera. Hence the actual scene depth map  $d_a$  is defined as follows:

$$d_a(x) = D_\infty \times (d(x) + d_0) \quad (33)$$

where  $D_\infty$  is a scaling constant for transforming the relative distance to the real distance, which in this paper is set to 10. With the estimated  $d_a(x)$ , we can calculate the TM for the R-G-B channels as:

$$t^\lambda(x) = Nrer(\lambda)^{d_a(x)} \quad (34)$$

With the estimated  $d_a(x)$ , we can calculate the TMs for the R-G-B channels  $t_{ULAP}(x)$  based on Eq. (2), setting the  $Nrer(\lambda)$  for R, G, B light as 0.83, 0.95 and 0.97, respectively.

The TM estimation based on NUDCP in Eqs. (29) highly depends on the input pixel's intensity. As shown in Fig. 7(e), some near background regions having small values of R intensity, get bigger values of  $t(x)$ , and are considered as foreground. The ULAP mainly considers that the bigger difference between the value of G-B channels and the value of the R channel is the farther depth, which can be used to compensate

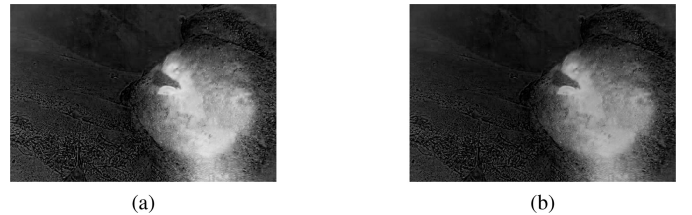


Fig. 8. The RSM and ARSM of the original of Fig. 7(f). (a) RSM obtained by Eq. (36); (b) ARSM obtained by Eq. (36), setting  $\lambda = 0.7$ .

and modify the TM estimation based on the NUDCP. The refined estimation of red channel  $t_{cps}^r(x)$  is computed as:

$$t_{cps}^r(x) = \sum_{i=1}^M \sum_{j=1}^N \min(t_{NUDCP}^r(i,j), t_{ULAP}^r(i,j)) \quad (35)$$

where  $M$  and  $N$  denote the width and height of the image, respectively. The minimum operation is used to adjust the overestimated TM due to the low intensity of the red channel when using the NUDCP.

So far, we have compensated the impact of the red channel in estimating the TM. We still have to take into consideration the influence of artificial light (AL). We found that the region with AL of Fig. 7(f) (where high intensities in the red channel exist in the green-bluish underwater image) has low saturation in the HSV color space. Saturation defined in Eq. (36), describes the purity of chromaticity of a pixel.

$$\begin{aligned} Sat(I^c(x)) &= \sum_{i=1}^M \sum_{j=1}^N \frac{\max(I^c(x)) - \min(I^c(x))}{\max(I^c(x))} \\ Sat(I^c(x)) &= 1, \text{ if } \max(I^c(x)) = 0 \end{aligned} \quad (36)$$

According to the HSV model, the very dark is fully saturated. A color will lose saturation when adding white light that contains power at all wavelengths. Hence, a region's lack of saturation in the image can be interpreted as a large amount of white light shooting in the region. Especially for underwater image, the saturation of the scene without AL is notably greater than that under artificially illuminated areas. We can express this phenomenon by a reversed saturation map (RMS) defined as Eq. (37). The region with high values of RMS often point to the AL affected region.

$$Sat^{rev}(x) = 1 - Sat(I^c(x)) \quad (37)$$

Then, we can use the RSM to optimize the estimated TM to reduce the effect of the artificial light. To modify relative values of the TM based on the reversed saturation, the  $\lambda \in [0, 1]$  is imported to the RSM as an effective scalar multiplier.

$$Sat_{adj}^{rev}(x) = \lambda * Sat^{rev}(x) \quad (38)$$

The RSM and ARSM of Fig. 7(f) are shown in Fig. 8. It can be seen that the areas under the scene of AL are segmented effectively from the rest of the image. Fig. 8(b) shows the adjusted RSM (ARSM) when the  $\lambda$  is set as 0.7. In the optimization of TM, we can change the values of the areas under artificial light using different values for  $\lambda$ .

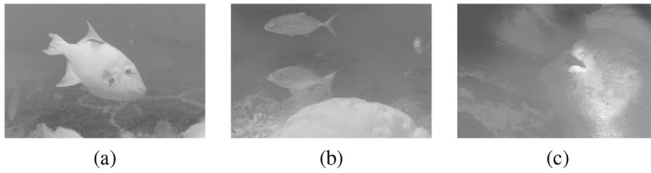


Fig. 9. Optimal TMs of the R channel for Fig. 7(d)–(f). (a) The white fish in the foreground scene is correctly estimated, with larger values closer to the camera; (b) the values of TM in the background scene are compensated by the depth map obtained based on the ULAP; (c) the TMs for the underwater image spotted by the AL have larger values for the scene points closer to the light and smaller values for the points farther from the light.

Using the ARSM, we can further modify the TM estimation by Eq. (39), which reduces the intensity of the artificial light region while preserving the intensity of other regions.

$$t_f^r(x) = \sum_{i=1}^M \sum_{j=1}^N \max(t_{cps}^r(i, j), Sat_{adj}^{rev}(i, j)) \quad (39)$$

By means of a series of compensation and modification processes on the NUDCP-based TM, the inaccurate TMs of Fig. 7(d)–(f) can be rectified. After being refined by the guided filter [48] and stretched by the histogram stretching, the final TMs are shown in Fig. 9.

Based on Eq. (2), the scene depth map is derived as

$$d(x) = \log_{Nrer(Red)} \left\{ t_f^r(x) \right\} \quad (40)$$

The TMs for the blue and green channels are computed based on the exponential relationship between normalized residual energy ratio  $Nrer(c')$  and the depth of object to the camera  $d(x)$ , and then deducted as Eq. (41):

$$t^{c'}(x) = Nrer(c')^{d(x)} \quad (41)$$

Because the estimated TMs are calculated over a local patch of the underwater image, some halos and block artifacts are produced in the transmission map  $t^c(x)$ . In order to solve these problems, the guided filter [48] is further used to refine the TMs.

Lastly, the recovered underwater image  $J^c$  is obtained by applying the refined TM and the estimated BL of the R-G-B channels into the Eq. (42):

$$J^c = \frac{I^c(x) - B^c}{\min(\max(t^c(x), 0.2), 0.9)} + B^c, \quad c \in \{r, g, b\} \quad (42)$$

where  $J^c$  is the restored underwater image. A lower bound and an upper bound for  $t^c(x)$  are empirically set to 0.2 and 0.9, respectively. We use one typical underwater image with artificial light [21] to demonstrate the outputs of the entire process of our method in Fig. 10. Fig. 10(b)–(d) show the TMs for red channel based NUDCP, the compensation of the depth map and the optimization of ARSM, and Fig. 10(e) shows the restored result. Fig. 10(f) obtained by color correction will be introduced in the next subsection.

### C. Color Correction

Although the underwater image can be dehazed by using restoration parameters of the TMs and BLs, the restored image is often characterized by low brightness and low contrast,

which veils many valuable image details. The proposed color correction is based on the white balance algorithm with optimal gain factor [33], [53] and can be described as:

$$\begin{cases} P_o = \frac{P_i}{\lambda_{max} \times (\mu/\mu_{ref}) + \lambda_v} \\ \mu_{ref} = \sqrt{(\mu_r)^2 + (\mu_g)^2 + (\mu_b)^2} \end{cases} \quad (43)$$

where  $P_o$  and  $P_i$  denote the color corrected image and the original underwater image.  $\mu_r, \mu_g, \mu_b$  represent the average value of each R-G-B channel of the input underwater image  $P_i$ , and  $\lambda_{max}$  is estimated by the maximum value of R-G-B channels of the input underwater image  $P_i$ . The value of  $\lambda_v$  is selected in the range of (0, 0.5) to get the desired color for the enhanced image. The closer  $\lambda_v$  is to 0, the lower the brightness of the corrected image is. Fig. 11 shows a selection of underwater images enhanced based on different values of  $\lambda_v$ .

Based on experimental results of many underwater images, we found that when the value of  $\lambda_v$  is 0.2, the corrected image is slightly brighter and when  $\lambda_v$  is 0.3 the corrected image is a little dim. Thus the optimal  $\lambda_v$  is chosen as 0.25 in this paper. Fig. 10(f) shows the enhanced result, which preserves the image details and improves visibility and contrast of the restored image.

## IV. RESULTS AND EVALUATION

In this section, to ensure the fairness of each evaluation, all the underwater images under test are pre-processed, setting the same resolution of  $400 \times 600$  pixels. All methods are implemented on a Windows 7 PC with Intel Core i7-4790U CPU@3.60GHz, 8.00GB 1600MHz DDR3 Memory, running Python3.6.3.

### A. Evaluation of Objectives and Approaches

We have conducted experiments on four objectives:

- a) To examine the effectiveness of the proposed MABLs;
- b) To assess the performance of the statistical BL model;
- c) To assess the performance of the TM optimizer;
- d) To assess the overall performance of the proposed underwater image enhancement method.

We carried out the evaluations by comparing with multiple underwater image restoration/enhancement methods. These methods include: Maximum Intensity Prior (MIP) [31], Dark Channel Prior (DCP) [18], [19], underwater image enhancement with a new optical model [54], Underwater Dark Channel Prior (UDCP) [22] (extended in [23]), depth estimation based on blurriness [27], Red channel [24], Li's method [25] and Peng's method based on image blurriness and light absorption [28]. In the interest of clarity, we present herein a comparative evaluation among the most representative methods, which are DCP [18], MIP [31], UDCP [22], Li's [25], and Peng's [28].

To objectively evaluate the performance of various underwater image restoration/enhancement methods from different aspects, we employed five image quality metrics, plus the running time (RT). The five quantitative metrics include two full-reference metrics (the root mean square error (RMSE) and the structural similarity (SSIM) [55]) and three non-reference

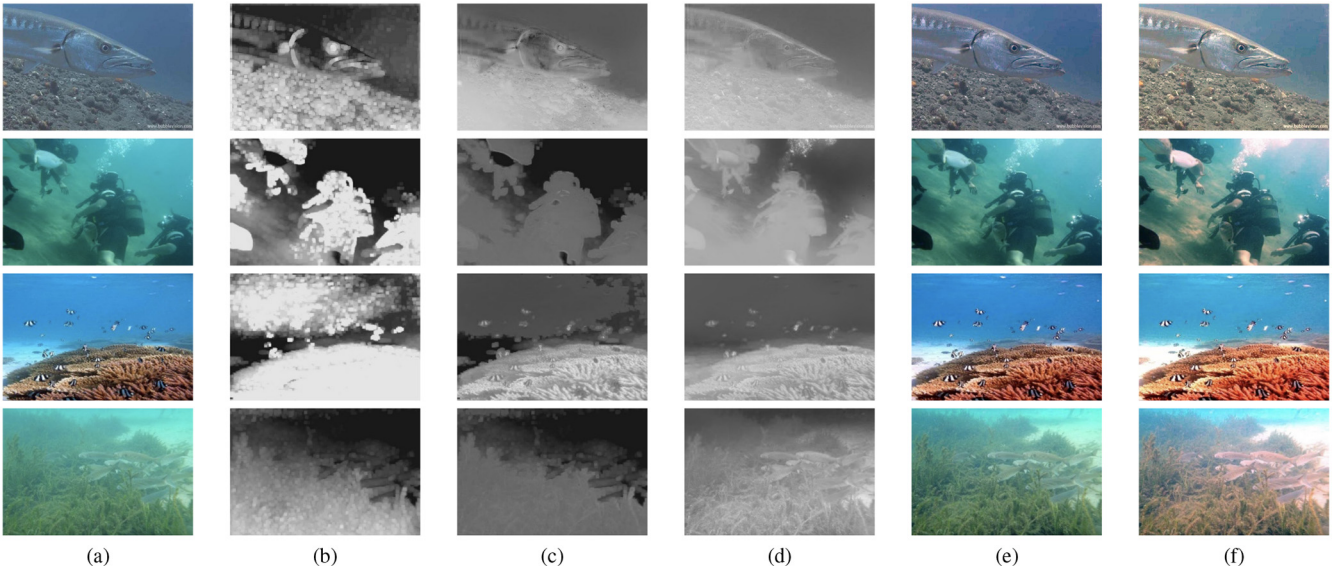


Fig. 10. The entire processing of underwater image enhancement. (a) Original underwater image; (b) coarse TM of the red channel obtained by NUDCP; (c) refined TM of the red channel compensated by TM of the red channel, estimated by ULAP; (d) refined TM of the red channel modified by the reversed saturation; (e) restored image; (f) enhanced image by color correction.

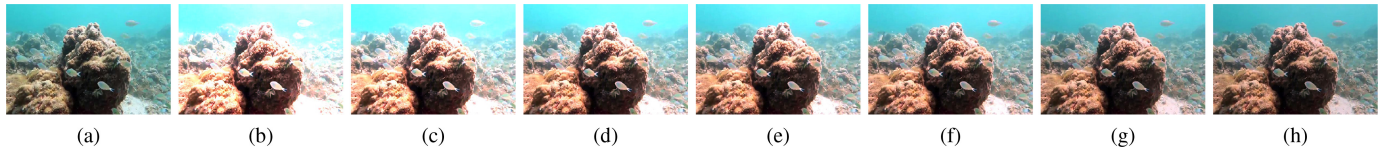


Fig. 11. Results of color correction based on different values of  $\lambda_v$ . (a) Original image; (b)–(h) the enhanced images with  $\lambda_v$  equal to 0, 0.1, 0.2, 0.25, 0.3, 0.4, and 0.5 respectively.

quantitative metrics (Entropy (S), the Blind/Referenceless Image Spatial Quality Evaluator (BRISQUE) [56], and Underwater color image-quality evaluation (UCIQE) [7]).

The RMSE metric mainly measures the degree of noise in the image. A smaller RMSE indicates better performance and vice versa. The SSIM metric is the most prominent approach introduced to evaluate the ability to preserve the structural information of the images. A higher SSIM represents high similarity between the dehazed image and the ground truth image and vice versa. Although RMSE and SSIM require the original underwater image as the reference image, they are still useful to indicate the introduced artificial noise of the enhanced image and the retention of structural information of the original image.

Entropy represents the abundance of information. A higher entropy value of an image states more valuable information contained in the image. The BRISQUE quantifies possible losses of naturalness in an image due to the presence of distortions. The BRISQUE value indicates the image quality from 0 (best) to 100 (worst). The UCIQE in a linear combination of chroma, saturation, and contrast evaluates the degree of the non-uniform color cast, blurring, and low-contrast in the underwater image. The quality level is represented in the range (0, 1), the higher, the better.

#### B. Effectiveness of Proposed MABLs

According to the principle of choosing the far scene points with high intensity and the most significant difference of R

channel and G-B channels, a manually annotated background lights (MABLs) database has been established with 500 underwater images. But a question is: are the MABLs proper? To answer this question, we conducted a series of experiments to use the MABLs and the BLs generated by the methods of DCP, MIP, UDCP, Li's method, Peng's method and our proposed method to restore the 500 underwater images based on IFM, under the same TMs. Then, we evaluated the restored image qualities under different BLs. Our assumption was: the highest quality would be seen on the images restored with the MABLs.

To avoid the influence of TMs, we adopted and improved the TMs from Peng's method [28] that is based on the light absorption and image blurriness for all the experiments. Some transmission maps with obvious estimation errors (e.g., a close-up fish is black in the map) were discarded, and 100 fully-proper transmission maps were chosen by the final manual selection. Table II gives the quality assessment results. It can be seen that, for all five quality assessment metrics, MABLs achieves the best performance.

Fig. 12 show different kinds of underwater image examples restored by using MABLs. Besides Peng's TMs, we also conducted the experiments under other TMs proposed in MIP, UDCP and Li's method. The results indicated the MABLs always performed the best, though the final results had different brightness or color tones.

It should be noticed that we cannot guarantee the absolute correctness of MABLs. For some images with a close shot,

TABLE II

QUANTITATIVE ANALYSIS VIA RMSE, SSIM, ENTROPY, BRISQUE, UCIQE AND RT OF RESTORATION RESULTS BASED ON DIFFERENT BLs AND THE SAME TMs [28]

Methods	Indexes					
	RMSE	SSIM	S	BRISQUE	UCIQE	RT (s)
DCP	39.12	0.52	6.72	34.05	0.32	0.92
MIP	36.38	0.53	6.64	33.14	0.36	1.97
UDCP	35.95	0.55	6.71	33.62	0.38	0.73
Li	28.57	0.76	7.36	29.55	0.46	1.48
Peng	31.62	0.71	6.98	30.37	0.41	1.55
Ours	23.64	0.81	7.67	28.56	0.49	<b>0.06</b>
MABLs	<b>21.99</b>	<b>0.83</b>	<b>7.88</b>	<b>28.15</b>	<b>0.53</b>	-

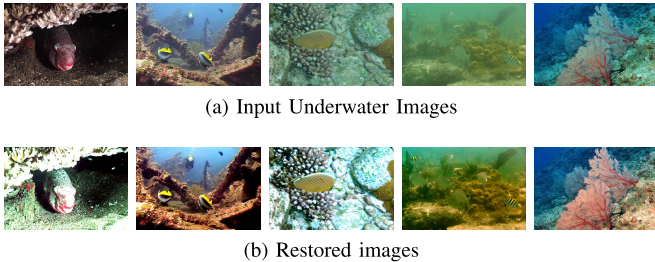


Fig. 12. Successful results based on the MABLs with the TMs [28].

the far scene point is difficult to identify. Thus, the MABLs may not work out a significant improvement of quality. Yet, we have found them not to cause any distortions. On the other hand, none of the BL estimation methods was effective in the experiments reported herein.

### C. Statistical Model of BL Estimation

1) *Discussion on BL Accuracy and Efficiency:* We applied the established statistical models to estimate the BLs of 30% of testing data of the MABLs database. Then, we computed the differences between the predicted BLs and the MABLs. Finally, we labeled the images when each predicted BL was accurate with a tolerant range of 30 for the R channel and 40 for the G-B channels. The tolerance was set because MABLs do have uncertainty to some extend and a small deviation of BLs does not have a great impact on the quality of restored images based on our experiments. The same labelling work has done on the BLs predicted by DCP, MIP, UDCP, Li's and Peng's methods. The compared results of prediction accuracy and running times are shown in Fig. 13.

From Fig. 13(a), the accuracy of BLs estimated by DCP and UDCP are the two lowest of all methods, showing that these are not always suitable for underwater image restoration. The overall prediction accuracy of the other three methods is clearly lower than our proposed statistical model.

We can see from Fig. 13(b) that the running time of DCP, UDCP, Peng's method and Li's method increases rapidly with image size, due to the pixel-by-pixel computation in the dark G-B or R-G-B channels. The running time of MIP is the longest one, because the maximum intensity is used twice to get the maximum intensity of the R channel and the maximum intensity of G-B channels. Our non-linear model for the R channel and linear model for G-B channels only need limited time to determine the BLs. The time efficiency can also

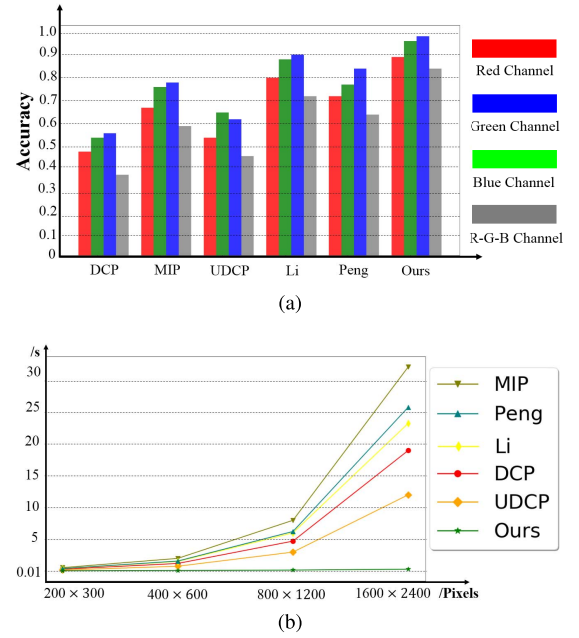


Fig. 13. (a) Accuracy of the estimated BLs with reference to MABLs; (b) running times (/s) with different sizes (/pixels) of test underwater images.

been seen from Table II, where our method is over 10 time faster than the fastest UDCP among other methods.

2) *Restoration of Images Based on the Statistical BL Model:* Fig. 14 demonstrates the restored images captured in sunlight and diving scenes, with the same TMs computed by the improved Peng's method. The DCP and UDCP methods for estimating BLs in Fig. 14(b) and (d) fail to improve the contrast and color. They even cause server distortion, which indicates that these methods cannot obtain the correct BLs of underwater images under these challenging scenes. The method proposed by Li (Fig. 14(e)) can produce nearly similar satisfactory results with the MIP method (Fig. 14(c)) because their BL estimation is based on the maximum difference between the R channel and the G-B channels. However, for the diver image under deep water, the restored images by Li's and Peng's method are relatively dimmer than the original image due to estimating the bigger BLs. Yet, our proposed BLs estimation can successfully improve both color and contrast, and the restored images appear with a range of different colors.

### D. Performance of Transmission Map Optimizer

Since the above experimental results have adequately demonstrated that the MABLs are best suitable for various underwater image restorations, we examined the performance of TM estimations based on the MABLs. Fig. 15 shows the restored images using different TMs. On account of DCP, MIP and UDCP methods generating a single TM for all R, G and B channels, they ignore the crucial difference between the TM of the R channel and the TMs of the G-B channels. As a result, in the restored coral and fish images some over-saturation areas are visible in Fig. 15(b-d).

From Fig. 15(e) and (f), the TMs obtained by Peng's and our method can increase the valuable image information, complete contrast, and local details. To conclude, the R and

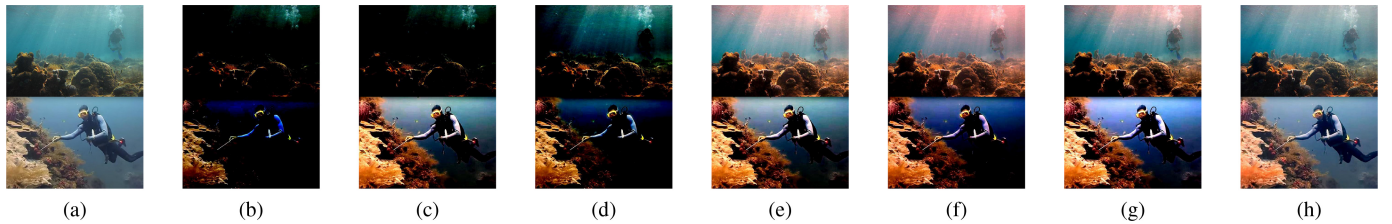


Fig. 14. Results with different color tones based on different BLs and the same TM. (a) Input images. (b)–(i) Restored results with different BLs proposed by (b) DCP, (c) MIP, (d) UDCP, (e) Li, (f) Peng, (g) Ours, (h) MABLs.

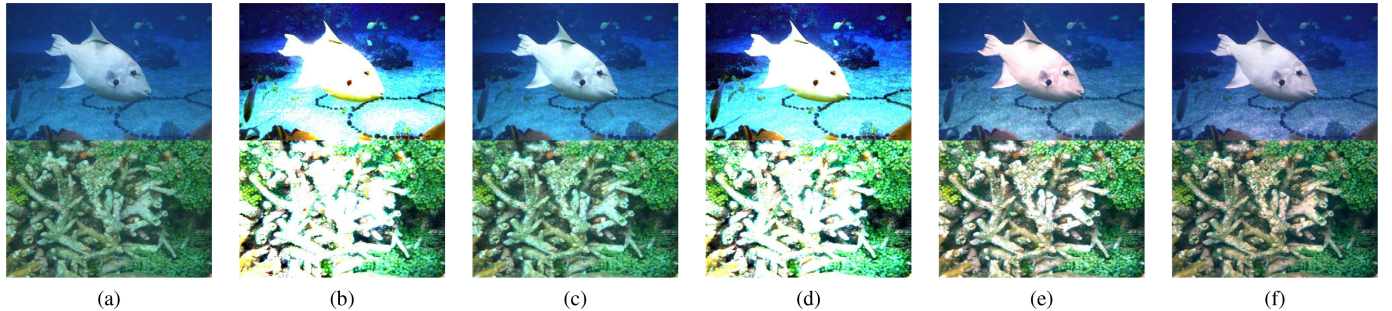


Fig. 15. Comparative results of restored images, with different TMs based on the MABLs. (a) Original images. The restored results by (b) DCP, (c) MIP, (d) UDCP, (e) Peng, (f) Ours.

TABLE III  
QUANTITATIVE ANALYSIS VIA RMSE, SSIM, ENTROPY, BRISQUE,  
UCIQE AND RT OF RESTORATION RESULTS BASED ON DIFFERENT  
ESTIMATED TMs AND MABLs

Methods	RMSE	SSIM	S	Indexes		
				BRISQUE	UCIQE	RT (s)
DCP	35.95	0.50	6.83	33.91	0.37	0.63
MIP	34.76	0.53	6.86	32.45	0.39	1.38
UDCP	30.11	0.51	6.98	31.71	0.42	<b>0.59</b>
Li	26.18	0.79	7.83	29.13	0.49	0.93
Peng	23.64	<b>0.82</b>	7.97	<b>28.27</b>	0.53	1.24
Ours	<b>22.31</b>	0.81	<b>7.99</b>	28.56	<b>0.54</b>	0.67

G-B TMs should be deducted from the characteristics of the corresponding channel separately.

From the full-reference and non-reference quality analyses of Table III, the results of DCP, MIP, and UDCP methods are remarkably poorer than the results achieved by ours and by Peng's methods. Although the results of Peng's method are slightly better than ours regarding SSIM and BRISQUE, the computational time of Peng's is nearly double.

#### E. Overall Performance of the Proposed Method

The objective of the proposed underwater image enhancement method was not only to recover the underlying scene radiance but also to enhance the contrast of underwater images, to preserve the genuine colors and to improve the visibility of the input images. Therefore, a color correction with white balance was added after restoration. To fairly evaluate the overall performance of our method, we compared our method with the IFM based methods DCP, MIP, UDCP, Peng's, as well as these methods with a post-processing of histogram equalization (HE). We also compared with Li's method [25], which introduces the red channel correction and adaptive exposure map estimation as color correction. For

TABLE IV  
QUANTITATIVE ANALYSIS VIA RMSE, SSIM, ENTROPY, BRISQUE,  
UCIQE AND RT OF RESTORATION AND ENHANCEMENT RESULTS BASED  
ON DIFFERENT METHODS

Methods	RMSE	SSIM	S	Indexes		
				BRISQUE	UCIQE	RT (s)
DCP	45.12	0.48	5.57	48.05	0.29	1.46
MIP	43.95	0.49	6.21	46.28	0.32	2.58
UDCP	47.56	0.56	5.81	41.18	0.34	1.02
Peng	30.59	0.71	7.38	35.78	0.52	2.21
OWCC	30.45	0.72	7.66	34.59	0.54	<b>0.69</b>
Li	32.45	0.68	7.42	35.73	0.52	1.86
DCP+HE	37.59	0.51	6.64	44.12	0.43	1.52
MIP+HE	38.82	0.58	6.81	43.88	0.46	1.61
UDCP+HE	39.28	0.58	6.71	37.78	0.47	1.13
Peng+HE	28.81	0.73	7.74	33.58	0.58	2.33
Ours	<b>27.45</b>	<b>0.75</b>	<b>8.03</b>	<b>31.78</b>	<b>0.63</b>	0.71

convenience, we named our image restoration without color correction as OWCC, and the full underwater enhancement method as Ours.

The quantitative assessments and running times are shown in Table IV, presenting the average values of 150 test images from the MBALs Database. Fig. 16 shows two examples of the comparative results. From Table IV, we can see that adding HE to the methods of DCP, MIP, UDCP and Peng's brings significant improvement of quality assessment at the cost of a slight increase in running times.

The impact of color correction can be observed in Fig. 16, by comparing the top images with the bottom images for the corresponding methods. The IFM-based image restoration methods (DCP, MIP, UDCP, Peng's) often fail to remove the greenish-bluish color. In particular, a greenish color still exists in the restored archaeology images. The color corrections have improved brightness, color and contrast, and effectively reduced the greenish. However, the restored underwater images enhanced by HE are over-saturated as the image

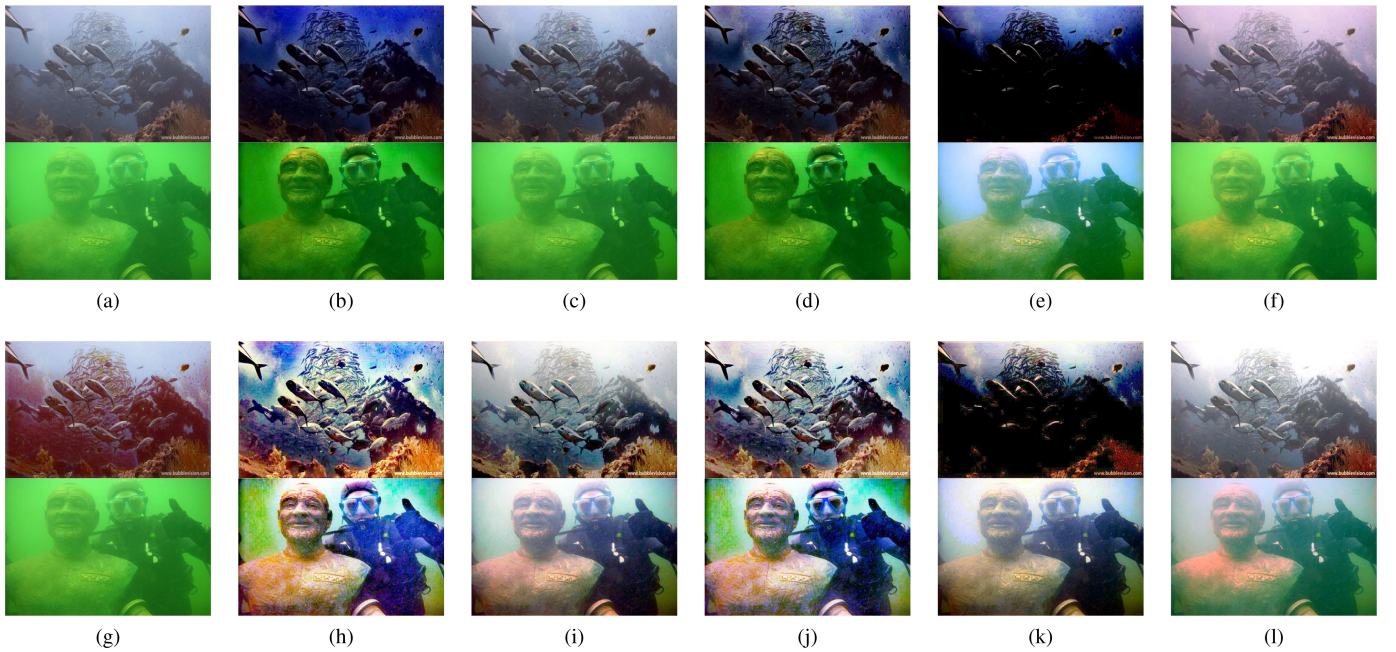


Fig. 16. Comparative results. (a) Original images, (b) DCP, (c) MIP, (d) UDCP, (e) Peng, (f) OWCC, (g) Li, (h) DCP+HE, (i) MIP+HE, (j) UDCP+HE, (k) Peng+HE, (l) Ours.

becomes too bright and unnatural, which also reduces the image valuable details, as shown in Fig. 16 (h–j).

The color correction may have negative effects. As shown in Fig. 16(k), the fish school is dimmer than the original image and even cannot be classified from the background scene. Our restoration method can effectively reduce the effect of light absorption and scattering, shown in Fig. 16 (f). The final images enhanced by the improved color correction, shown in Fig. 16 (l), considering the special characteristics of each R-G-B channel and the relation of RGB three color channels, are neither over-saturated nor over-enhanced, wherein the objects are better differentiated from the background.

To sum up, the effect of greenish illumination remains in the output images produced by physical-based methods. It is necessary to introduce a proper color correction to remove some blue-green illumination, and improve the color and saturation of the input image.

## V. DISCUSSION

We have proposed an underwater image enhancement method that includes two processes: 1) underwater image restoration, based on novel statistical models of BLs estimation and optimal TM estimation models; and 2) a simple color correction based on white balancing, using the optimal gain factor.

The accuracy of the estimated BLs and TMs influences the restored quality of underwater images based on the image formation model. Meanwhile the accuracy of the BLs affects the estimation of the TMs. Hence, an effective BL estimation model is the premise of successful TM estimation and underwater image restoration. To demonstrate that our proposed method can recover and enhance the quality of different underwater images, and achieve similar results to those obtained using learning-based methods, we applied our

proposed method to images including challenging underwater scenes, offering a comparison with other restoration methods based on the CNN.

### A. Enhanced Images With Challenging Underwater Scenes

We selected several different challenging scenes, including greenish scenes, bluish scenes, thickly hazy scenes, low-visibility background scenes, turbid scenes, and low-visibility scenes (first row of Fig. 17). The corresponding estimated BLs, TMs of the red channel, and enhanced images are shown in the second, the third and the fourth rows, respectively.

In Fig. 17(a–e), our statistical model of BL estimation can successfully estimate the global background light of the entire scene, avoiding the interference of the white block or bright point in the foreground object. The estimated TMs are also reasonable, whereby the farther the object is from the camera, the darker the TMs is. In the enhanced images, the white balancing with optimal gain factor is essential to be introduced to improve the color and contrast of the restored images because the restoration method can only remove the haze and blur of the original image.

### B. Comparison With Restoration Methods Based on the CNN

Reference [33] and our proposed method have different experimental conditions. The deep learning CNN needs to be trained with a vast amount of data, which makes it difficult to fully replicate. To compare, we extracted some representative underwater images presented in [33], giving the results processed by our proposed method. Original images, results from [33], and our results are shown in Fig. 18. Although the original images directly cropped from the article [33] have low resolution, from the compared results, we can spot that our proposed method with lower running time can be well-suited

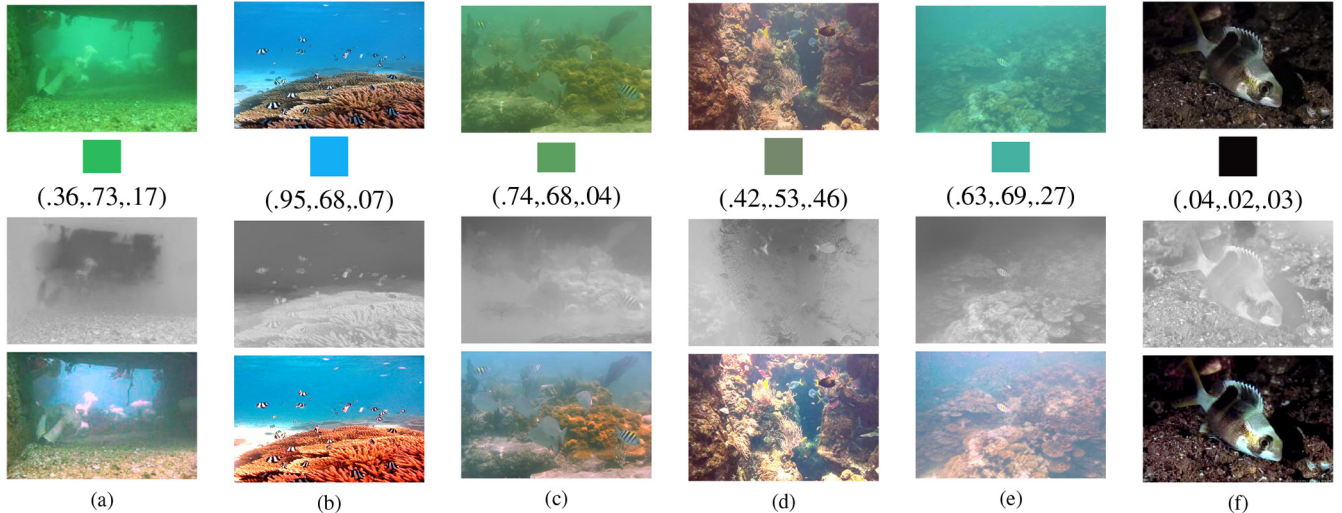


Fig. 17. Enhanced results. (a) Coarse image with greenish scene, (b) Coarse image with bluish scene, (c) Shoal of fish with thickly hazy scene, (d) Underwater chasm image with low-visibility background scene, (e) Turbid image with the severe distortion, (f) Fish image under a dim scene.

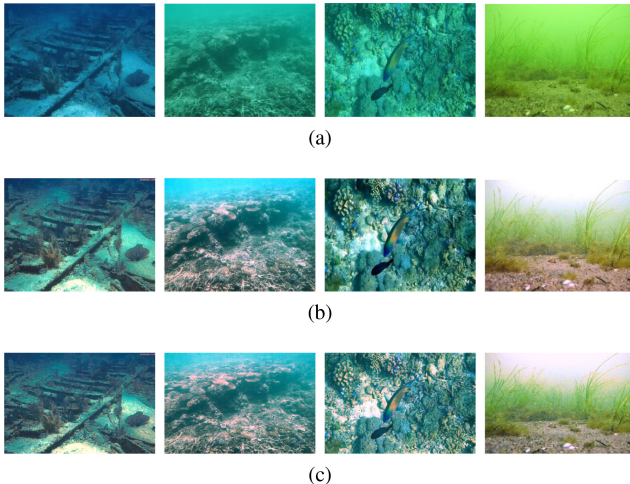


Fig. 18. Comparison results. (a) Original images, (b) Ding's method [33], (c) Ours.

to different underwater images enhancements, in terms of both high contrast and good visibility.

## VI. CONCLUSION

We have proposed an underwater image enhancement method including underwater image restoration, based on novel statistical models of BLs estimation and optimal TM estimation models, and a simple color correction based on improved white balance. To guarantee the robustness and high accuracy of BL estimation model, we established a first MABLs database, providing a statistical analysis on the histogram distribution of R and G-B channels separately, referring to the MABLs. The TM of the R channel was estimated based on the NUDCP, further compensated by the depth map and modified by the ARSM. The TMs of G-B channels were deducted according to the optical properties of the underwater image formation. Simple yet effective color correction was introduced to improve the

contrast and color of the restored images. The MABLs database and the code of the proposed method are accessible from <https://github.com/wangyanckxx/Enhancement-of-Underwater-Images-with-Statistical-Model-of-BL-and-Optimization-of-TM>.

Our comparative evaluation demonstrates the effectiveness of the MABLs, the high accuracy of our BLs estimation model, the rationality and low-complexity of our TMs estimation model, and the superior performance of our proposed image enhancement model. Our method has better results in processing various underwater images. Nevertheless, it was not possible to estimate accurate BLs for some images including close-shot objects, partially due to the limitation of manual annotation of BLs based on the far scene. However, these type of images are not sensitive to the BLs in the process of restoration, and thus our method does not exert any additional distortions on the original image.

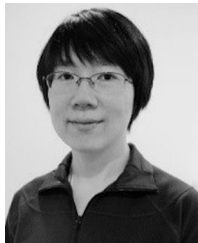
Compared to the recent ground-truth dataset of scene distance maps, which was produced from stereo cameras [40], our transmission map estimation is limited to recovering underwater images with no or little red component. This is because our TM estimation relies on the information of the red channel. In future work, we will continue to optimize the statistical BL estimation model and the TMs estimation model.

## REFERENCES

- [1] H. Z. Nafchi and M. Cheriet, "Efficient no-reference quality assessment and classification model for contrast distorted images," *IEEE Trans. Broadcast.*, vol. 64, no. 2, pp. 518–523, Jun. 2018.
- [2] E. Trucco and A. T. Olmos-Antillon, "Self-tuning underwater image restoration," *IEEE J. Ocean. Eng.*, vol. 31, no. 2, pp. 511–519, Apr. 2006.
- [3] C. D. Mobley, "Radiative transfer in the ocean," in *Encyclopedia of Ocean Sciences*. Cambridge, U.K.: Cambridge Univ. Press, 2013, pp. 619–628.
- [4] B. L. McGlamery, "A computer model for underwater camera systems," in *Proc. SPIE*, Mar. 1980, Art. no. 208.
- [5] J. Jaffe, "Computer modeling and the design of optimal underwater imaging systems," *IEEE J. Ocean. Eng.*, vol. 15, no. 2, pp. 101–111, Apr. 1990.

- [6] R. Schettini and S. Corchs, "Underwater image processing: State of the art of restoration and image enhancement methods," *EURASIP J. Adv. Signal Process.*, vol. 2010, no. 1, Apr. 2010, Art. no. 746052, doi: [10.1155/2010/746052](https://doi.org/10.1155/2010/746052).
- [7] M. Yang and A. Sowmya, "An underwater color image quality evaluation metric," *IEEE Trans. Image Process.*, vol. 24, no. 12, pp. 6062–6071, Dec. 2015.
- [8] X. Min, G. Zhai, K. Gu, Y. Liu, and X. Yang, "Blind image quality estimation via distortion aggravation," *IEEE Trans. Broadcast.*, vol. 64, no. 2, pp. 508–517, Jun. 2018.
- [9] M. T. Vega, C. Perra, F. De Turck, and A. Liotta, "A review of predictive quality of experience management in video streaming services," *IEEE Trans. Broadcast.*, vol. 64, no. 2, pp. 432–445, Jun. 2018.
- [10] Y. Wang, W. Song, G. Fortino, L. Qi, W. Zhang, and A. Liotta, "An experimental-based review of image enhancement and image restoration methods for underwater imaging," *IEEE Access*, vol. 7, pp. 140233–140251, 2019.
- [11] K. Zuiderveld, "Contrast limited adaptive histogram equalization," in *Graphics Gems*. Boston, MA, USA: Elsevier, 1994, pp. 474–485.
- [12] M. S. Hitam, E. A. Awalludin, W. N. J. H. W. Yussof, and Z. Bachok, "Mixture contrast limited adaptive histogram equalization for underwater image enhancement," in *Proc. Int. Conf. Comput. Appl. Technol. (ICCAT)*, Jan. 2013, pp. 1–5.
- [13] K. Iqbal, R. A. Salam, A. Osman, and A. Z. Talib, "Underwater image enhancement using an integrated colour model," *IAENG Int. J. Comput. Sci.*, vol. 34, no. 2, pp. 1–6, Jan. 2007.
- [14] K. Iqbal, M. O. Odetayo, A. E. James, R. A. Salam, and A. Z. H. Talib, "Enhancing the low quality images using unsupervised colour correction method," in *Proc. IEEE Int. Conf. Syst. Man Cybern.*, Oct. 2010, pp. 1703–1709.
- [15] C. Ancuti, C. O. Ancuti, T. Haber, and P. Bekaert, "Enhancing underwater images and videos by fusion," in *Proc. IEEE Conf. Comput. Vis. Pattern Recognit.*, Jun. 2012, pp. 81–88.
- [16] A. S. A. Ghani and N. A. M. Isa, "Underwater image quality enhancement through integrated color model with Rayleigh distribution," *Appl. Soft Comput.*, vol. 27, pp. 219–230, Feb. 2015.
- [17] A. S. A. Ghani and N. A. M. Isa, "Automatic system for improving underwater image contrast and color through recursive adaptive histogram modification," *Comput. Electron. Agricult.*, vol. 141, pp. 181–195, Sep. 2017.
- [18] K. He, J. Sun, and X. Tang, "Single image haze removal using dark channel prior," *IEEE Trans. Pattern Anal. Mach. Intell.*, vol. 33, no. 12, pp. 2341–2353, Dec. 2011.
- [19] L. Chao and M. Wang, "Removal of water scattering," in *Proc. IEEE 2nd Int. Conf. Comput. Eng. Technol.*, 2010, pp. 35–39.
- [20] H.-Y. Yang, P.-Y. Chen, C.-C. Huang, Y.-Z. Zhuang, and Y.-H. Shiao, "Low complexity underwater image enhancement based on dark channel prior," in *Proc. IEEE 2nd Int. Conf. Innov. Bioinspired Comput. Appl.*, Dec. 2011.
- [21] J. Y. Chiang and Y.-C. Chen, "Underwater image enhancement by wavelength compensation and dehazing," *IEEE Trans. Image Process.*, vol. 21, no. 4, pp. 1756–1769, Apr. 2012.
- [22] P. Drews, Jr., E. do Nascimento, F. Moraes, S. S. C. Botelho, and M. F. M. Campos, "Transmission estimation in underwater single images," in *Proc. IEEE Int. Conf. Comput. Vis. Workshops*, Dec. 2013, pp. 825–830.
- [23] P. L. J. Drews, E. R. Nascimento, S. S. C. Botelho, and M. F. M. Campos, "Underwater depth estimation and image restoration based on single images," *IEEE Comput. Graph. Appl.*, vol. 36, no. 2, pp. 24–35, Mar/Apr. 2016.
- [24] A. Galdran, D. Pardo, A. Picón, and A. Alvarez-Gila, "Automatic red-channel underwater image restoration," *J. Vis. Commun. Image Represent.*, vol. 26, pp. 132–145, Jan. 2015.
- [25] C. Li, J. Quo, Y. Pang, S. Chen, and J. Wang, "Single underwater image restoration by blue–green channels dehazing and red channel correction," in *Proc. IEEE Int. Conf. Acoust. Speech Signal Process. (ICASSP)*, Mar. 2016, pp. 1731–1735.
- [26] C.-Y. Li, J.-C. Guo, R.-M. Cong, Y.-W. Pang, and B. Wang, "Underwater image enhancement by dehazing with minimum information loss and histogram distribution prior," *IEEE Trans. Image Process.*, vol. 25, no. 12, pp. 5664–5677, Dec. 2016.
- [27] Y.-T. Peng, X. Zhao, and P. C. Cosman, "Single underwater image enhancement using depth estimation based on blurriness," in *Proc. IEEE Int. Conf. Image Process. (ICIP)*, Sep. 2015, pp. 4952–4956.
- [28] Y.-T. Peng and P. C. Cosman, "Underwater image restoration based on image blurriness and light absorption," *IEEE Trans. Image Process.*, vol. 26, no. 4, pp. 1579–1594, Apr. 2017.
- [29] Y. Wang, H. Liu, and L.-P. Chau, "Single underwater image restoration using adaptive attenuation-curve prior," *IEEE Trans. Circuits Syst. I, Reg. Papers*, vol. 65, no. 3, pp. 992–1002, Mar. 2018.
- [30] K. Zhang, W. Zuo, Y. Chen, D. Meng, and L. Zhang, "Beyond a Gaussian denoiser: Residual learning of deep CNN for image denoising," *IEEE Trans. Image Process.*, vol. 26, no. 7, pp. 3142–3155, Jul. 2017.
- [31] N. Carlevaris-Bianco, A. Mohan, and R. M. Eustice, "Initial results in underwater single image dehazing," in *Proc. OCEANS MTS/IEEE SEATTLE*, Sep. 2010, pp. 1–8.
- [32] X. Liu, G. Zhong, C. Liu, and J. Dong, "Underwater image color constancy based on DSNMF," *IET Image Process.*, vol. 11, no. 1, pp. 1–5, Jan. 2017.
- [33] X. Ding, Y. Wang, J. Zhang, and X. Fu, "Underwater image dehaze using scene depth estimation with adaptive color correction," in *Proc. IEEE OCEANS Aberdeen*, Jun. 2017, pp. 1–5.
- [34] X. Ding, Y. Wang, Z. Liang, J. Zhang, and X. Fu, "Towards underwater image enhancement using super-resolution convolutional neural networks," in *Proc. Int. Conf. Internet Multimedia Comput. Service*, 2017, pp. 479–486.
- [35] K. Cao, Y.-T. Peng, and P. C. Cosman, "Underwater image restoration using deep networks to estimate background light and scene depth," in *Proc. IEEE Southwest Symp. Image Anal. Interpretation (SSIAI)*, Apr. 2018, pp. 1–4.
- [36] D. Eigen, C. Puhrsch, and R. Fergus, "Depth map prediction from a single image using a multi-scale deep network," in *Proc. Adv. Neural Inf. Process. Syst.*, 2014, pp. 2366–2374.
- [37] D. Yang and J. Sun, "Proximal dehaze-net: A prior learning-based deep network for single image dehazing," in *Proc. Comput. Vision ECCV*, 2018, pp. 729–746.
- [38] J. Zhang *et al.*, "Dynamic scene deblurring using spatially variant recurrent neural networks," in *Proc. IEEE Conf. Comput. Vis. Pattern Recognit. (CVPR)*, Jun. 2018, pp. 2521–2529.
- [39] C. Li *et al.*, "An underwater image enhancement benchmark dataset and beyond," *arXiv: 1901.05495 [cs]*, Jan. 2019.
- [40] D. Berman, D. Levy, S. Avidan, and T. Treibitz, "Underwater single image color restoration using haze-lines and a new quantitative dataset," *arXiv: 1811.01343 [cs]*, Nov. 2018.
- [41] S. G. Narasimhan and S. K. Nayar, "Chromatic framework for vision in bad weather," in *Proc. IEEE Conf. Comput. Vis. Pattern Recognit. (CVPR)*, 2000, pp. 1598–1605.
- [42] R. Fattal, "Single image dehazing," in *Proc. ACM SIGGRAPH*, 2008, pp. 1985–1998.
- [43] S. G. Narasimhan and S. K. Nayar, "Vision and the atmosphere," *Int. J. Comput. Vis.*, vol. 48, no. 3, pp. 233–254, Jul. 2002.
- [44] R. T. Tan, "Visibility in bad weather from a single image," in *Proc. IEEE Conf. Comput. Vis. Pattern Recognit.*, Jun. 2008, pp. 1–8.
- [45] X. Zhao, T. Jin, and S. Qu, "Deriving inherent optical properties from background color and underwater image enhancement," *Ocean Eng.*, vol. 94, pp. 163–172, Jan. 2015.
- [46] S. Serikawa and H. Lu, "Underwater image dehazing using joint trilateral filter," *Comput. Elect. Eng.*, vol. 40, no. 1, pp. 41–50, Jan. 2014.
- [47] H. Liu and L.-P. Chau, "Underwater image restoration based on contrast enhancement," in *Proc. IEEE Int. Conf. Digit. Signal Process.*, 2017, pp. 584–588.
- [48] K. He, J. Sun, and X. Tang, "Guided image filtering," *IEEE Trans. Pattern Anal. Mach. Intell.*, vol. 35, no. 6, pp. 1397–1409, Jun. 2013.
- [49] S. Q. Duntley, "Light in the sea," *J. Opt. Soc. America*, vol. 53, no. 2, p. 214, Feb. 1963.
- [50] C. Li, J. Guo, B. Wang, R. Cong, Y. Zhang, and J. Wang, "Single underwater image enhancement based on color cast removal and visibility restoration," *J. Electron. Imag.*, vol. 25, no. 3, Jun. 2016, Art. no. 033012.
- [51] D. Huang, Y. Wang, W. Song, J. Sequeira, and S. Mavromatis, "Shallow-water image enhancement using relative global histogram stretching based on adaptive parameter acquisition," in *Proc. Int. Conf. Multimedia Model.*, 2018, pp. 453–465.
- [52] W. Song, Y. Wang, D. Huang, and D. Tjondronegoro, "A rapid scene depth estimation model based on underwater light attenuation prior for underwater image restoration," in *Advances in Multimedia Information Processing—PCM 2018*, R. Hong, W.-H. Cheng, T. Yamasaki, M. Wang, and C.-W. Ngo, Eds. Cham, Switzerland: Springer Int., 2018, pp. 678–688.
- [53] S. Hordley and G. Finlayson, "Re-evaluating colour constancy algorithms," in *Proc. 17th Int. Conf. Pattern Recognit. (ICPR)*, 2004, pp. 76–79.

- [54] H. Wen, Y. Tian, T. Huang, and W. Gao, "Single underwater image enhancement with a new optical model," in *Proc. IEEE Int. Symp. Circuits Syst. (ISCAS)*, May 2013, pp. 753–756.
- [55] Z. Wang, A. C. Bovik, H. R. Sheikh, and E. P. Simoncelli, "Image quality assessment: From error visibility to structural similarity," *IEEE Trans. Image Process.*, vol. 13, no. 4, pp. 600–612, Apr. 2004.
- [56] A. Mittal, A. K. Moorthy, and A. C. Bovik, "No-reference image quality assessment in the spatial domain," *IEEE Trans. Image Process.*, vol. 21, no. 12, pp. 4695–4708, Dec. 2012.



**Wei Song** (Member, IEEE) received the Ph.D. degree in computer science from the Queensland University of Technology, Brisbane, Australia, in 2012, where she was a Research Fellow from 2012 to 2015. In 2016, she became a Professor with Shanghai Ocean University, Shanghai, China, and a Special Professor (Eastern Scholar) with the Shanghai Institutions of Higher Learning, where she is a Co-Founder of the Joint Intellisensing Lab. Her research interests include image/video processing, machine learning, quality of experience modeling, and ocean big data analysis.



**Antonio Liotta** is a Professor with the Data Science and Intelligent Systems, Edinburgh Napier University, U.K., where he is a coordinating multi-disciplinary programs in Data Science and Artificial Intelligent. He was a Professor of data science and the Founding Director of the Data Science Research Centre, University of Derby, U.K. He has recently been awarded a Prestigious Fellowship in China, where he is the Founding Director of the Joint Intellisensing Lab and holds a Visiting Professorship with Shanghai Ocean University. He was leading all university-wide research, educational, and infrastructure programs in data science and artificial intelligence. His team is at the forefront of influential research in data science and artificial intelligence, specifically in the context of smart cities, Internet of Things, and smart sensing. He is renowned for his contributions to miniaturized machine learning, particularly in the context of the Internet of Things. He has led the international team that has recently made a breakthrough in artificial neural networks, using network science to accelerate the training process. He is the Editor-in-Chief of the *Internet of Things* (Springer); an Associate Editor of the *Journal of Network and Systems Management*, the *Indian Journal of Nuclear Medicine*, the *Journal of Micromechanics and Microengineering*, and *Information Fusion*; and an Editorial Board Member of six other journals.



**Yan Wang** is currently pursuing the Ph.D. degree with the Academy for Engineer and Technology, Fudan University, Shanghai, China. His current research focuses on computer vision, image processing, quality of experience, machine learning, and deep leaning.



**Cristian Perra** (Senior Member, IEEE) received the Ph.D. degree in electronic engineering and computer science from the University of Cagliari, Italy, in 2003, where he is a Professor of communications with the Department of Electrical and Electronic Engineering. He is serving as a Visiting Professor with Shanghai Ocean University, Shanghai, China. He is a Research Associate with the Multimedia Communications Laboratory, CNIT (National Inter-University Consortium for Telecommunications, Cagliari, Italy). He is the Co-Founder and a Member of the Management Team of the Joint Intellisensing Lab, an International Lab for transdisciplinary research in the area of intellisensing (a combination of artificial intelligence and smart sensing), joining expertise and facilities to achieve global impact of cutting-edge innovations. He is an expert member of the International Standard Organization ISO/IEC SC29 and Working Group WG1 (JPEG). His primary research interests include network applications and services, multimedia communications, signal processing, medical image processing, 2-D/3-D image and video coding and transmission, light field/holography/point cloud coding and transmission, virtual/augmented/mixed reality, sensor networks, applications for smart devices and smartphones, quality of experience, and quality of service for multimedia communications.



**Dongmei Huang** received the first M.E. degree in electrical and engineering from Xi'an Jiao Tong University, China, in 1985, and the second M.E. degree in industrial automation from Information Engineering University, China, in 1991. She is currently the Vice-Chancellor and a Professor with the Shanghai University of Electric Power, China. Her main research interests include marine informationization, data mining, and database technology.